TUNGSTEN INERT GAS (TIG) WELDING OF AUSTENITIC STAINLESS STEEL (ASS) : EXPERIMENTAL OF CHROMIUM CARBIDE FORMATION DURING TIG OF ASS 304L

B.T Balogun[1], B. Alkali[2] M. Abdulwahab [3] and Anunuso Justice Chikeze[2]

[1] Department of Materials and Metallurgical Engineering,
Federal University of Technology, Minna, Nigeria.

[2]Department of Mechatronics Engineering,
Federal University of Technology, Minna, Nigeria.

[3]Department of Metallurgical and Materials Engineering, Faculty of Engineering,
Ahmadu Bello University Zaria, Nigeria.
Emails: balogun.tope@futminna.edu.ng, +2347068364092.

Abstract

In this paper, a 230 x 150 x 5mm dimension of austenitic stainless steel (ASS) plates of type 304Lwas investigated to observe the formation of chromium carbide when wielding current and temperature were applied at a given period of time. The plates were joined using Tungsten Inert Gas (TIG) welding process. Various lower welding current were biased to obtain a range of desirable welding temperature without the formation of Chromium Carbide at a very lower welding current and temperature. The biased current ranges from 50A to 90A and the corresponding welding temperature were recorded using thermocouple device. The result of the macro-structure gives an interesting revelation of smallest dimension of width of 1.0mm and 1.2mm within the heat affected zone (HAZ) at lower temperature between 100.6^{o}C and 200.2^{o}C. These values indicate welded materials with better mechanical properties (hardness and strength). as compared to metals welded at higher temperature of 300.8^{o}C to 500.6^{o}C which gives a higher dimension of width between the ranges of 2.2mm to 3.2mm in HAZ. The metal with higher temperature between 300.8^{o}C and 500.6^{o}C shows lower mechanical properties (hardness and strength). The result of the micro-structures also reveals that, the material welded with the lowest temperature within the range of 100.6^{o}C and 200.2^{o}C exhibit no chromium carbide formation as compared to metals welded at higher temperature of 300.8^{o}C to 500.6^{o}C which establish the formation of chromium carbide in a weld of austenitic stainless steel. This result has proven that, at control weld current and temperature, the life span of the ASS 304L can be protected and chromium carbide formation that leads to weld decay can be avoided.

Keywords: Austenitic stainless steel; Macro-structure; Chromium Carbide; Gas inert Tungsten; Heat affected zone; Microstructure.

1.0 INTRODUCTION

Austenitic Stainless Steel (ASS) is widely used in high temperature corrosive environments. They exhibit superior corrosion resistance in a wide range of environments such as petrochemical and

nuclear industry where there is existence of hot gases and high boiling liquid. However, there have been great challenges of corrosion of different kinds confronting petrochemical and nuclear industries all over the world in the exploitation of ASS (Mishra et al., 2014). This is due to a specific corrosion mechanism called "weld decay" which influences the presence of Chromium Carbide formation during welding process. These challenges pose a great danger on the life span of welded materials of high quality such as ASS in petrochemicals and nuclear industries. When these welded materials are subjected to a specific corrosion mechanism such as "weld decay", it resulted to failure which limits the lifespan of such material (Mishra et al., 2014). Most especially when such material is practically used in the industry. This research work attempt to investigate at what particular welding current and welding temperature ASS 304L can be welded to avoid carbide formation that leads to "weld decay" in order to avoid the material prone to corrosion of all kinds.

A lot of researches have been done on the welding of ASS. The work of Roy et al. (2014) specifies the use of different electrode in a shield metal arc welding by exploring the mechanical and metallurgical properties of commercially pure Copper and ASS AISI 304. Among the electrodes used, it was observed that Inconel (NiCrMo3) electrode produces a better weld joint and strength. The suitability of (NiCrMo3) was recommended for industrial practice. The discovery made by Oyetunji et al. (2013), on the effects of welding speeds and power inputs on the hardness property of ASS 304L using GIT Arc welding, reveals formation of chromium carbide at post weld as well as high level of hardness at a faster welding speed of 9.5m/min and corresponding power input of 9.2KN. Tabish et al. (2014), investigated the effects of heat input on micro-structure and mechanical property using TIG in an ASS AISI 304. The research achieved high strength and hardness of material through a low heat input parameter when heat inputs were varied at low, medium and high conditions.

The research of Moslemi et al. (2015), on the effect of welding current on micro-structure and mechanical properties of ASS 316 in a welded joint using TIG, re-affirmed chromium carbide formation at weld joint due to increase in heat input. This established that increase in welding current causes a raise in heat input. It was also concluded that current of 100A is the most suitable current that gives optimal strength and hardness in welding of ASS AISI 304 using TIG welding process. Mishra et al. (2014), studied mechanical characterization of monel 400 and 316 of ASS weldments using Gas Tungsten arc welding (GTAW) and ERNiCrMo-3 filler metal. These researchers limits their areas of study to the welding technique of GTAW, a particular material monel 400 and a filler wire of ERNiCrMo-3 without considering the outcome of the evaluation of welding parameters such as current, heat input, temperature or voltage in the experiment. In their opinion, GTAW welding was recommended for weld monel 400 and AISI 316 of ASS using ERNiCrMo-3 filler wire. But the research work recorded tensile failure in all dissimilar weldments.

The mechanical properties of AISI 4140 and AISI 316 dissimilar weldments using GTAW with and without filler metal in an ASS were assessed by Raddy et al. (2014). The report indicated the present of martensite and also recorded tensile failure in both weldments. In a recent development, Song et al. (2017) investigated the effect of high – pressure H2 on the fracture behaviour of pipeline steel X70, ASS304L and ASS 316 type. It was discovered that 304L type of ASS is more susceptible to hydrogen brittleness than the ASS 316. A prediction model developed by Gao and Zhang (2014) on how the morphology of a molten welding pool width can be monitored and control in a laser welding process was achieved. This model predicts a high power disk laser

welding of ASS 304 using computer artificial intelligent device. Yang et al. (2010) studied effects of heat input on tensile properties and fracture behaviour of friction stir welded Mg-3Al-1Zn alloy, by stir welded 6.3mm thickness of the material. They established that the highest value of ultimate tensile strength of the weld was achieved with increase in heat input at shoulder diameter of 24mm. They were also affirmed that increase in the width of heat affected zone (HAZ) does not bring about increase in hardness value of the weld.

The research of Jao et al. (2016) on the effect of welding residual stress and out of plane displacement during the heat sink welding process of a thin stainless steel using computer artificial intelligent device (CAID) was tremendous. The simulation discovered that, a trailing heat sink welding has a little effects on the deformation. This is due to imposition of stress on material when there is a decrease in heat input in a conventional welding of stainless steel. The study of Mendes et al. (2013) on the influence of exposure characteristics on weld interfaces of stainless steel AISI 304L to low alloy steel (51CrV4) in a cylindrical configuration was achieved using ammonium nitrate-based emulsion and ammonium nitrate fuel (ANFO) explosives with the aid of CAID. The study affirmed that, the morphology of the welding pool was influenced by the velocity impact of the explosives used. It also ascertains that welding with ANFO explosives has a better configuration performance with both filler and base metal.
The success in optimization of deep penetration laser welding process of stainless steel using 10KW fibre laser was studied by Zhang et al; (2014). The study established that welding speed and focal position affects the quality of the weld in a laser welding process. The study also proves that, the magnitude of 10KW power in a fibre laser welding process improves the tensile strength of the material in ASS of 304 type. However, none of these researchers has considered at what applied current and particular temperature, does chromium carbide formation occurs in welding process of ASS. This paper investigates the welding current and a particular range of vibrant temperature at which ASS304L type can be welded without significant chromium carbide formations in the weld.

2.0 Methodology

The methodology comprises of three stages namely; the preparatory stage; the welding process and the metallurgical test as illustrated on Figure 1.

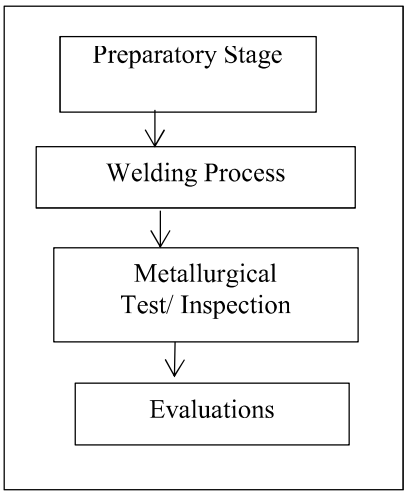

Figure 1: System Block Diagram

2.1 The Preparatory Stage

A dimension of 230mm x 150mm x 5mm thick sample of ASS 304L type of an appreciable length L was obtained. The sample was set up and cut into five (5) equal pieces of 60mm x 30mm x 5mm using power hack saw. The setup follows V-grooved butt configurations with a roof face of 1mm inclined at 30°C and the land face of 2mm. The edge of each cut pieces was thoroughly cleaned with emery cloth and methylated spirit. Chemical composition of as-received 304L austenitic stainless steel plate was studied by infrared ray emission photo spectrometry using Raman Infrared Spectrophotometer (RIS) material analyser as illustrated in Table 1 before the welding process was carried out.

Table 1: Chemical composition base metal 304L stainless steel.

Elements	C	Mn	P	S	Si	Cr	Ni	Mo	Fe
%wt	0.03	2.00	0.045	0.039	1.00	18.04	8.09	0.36	70.38

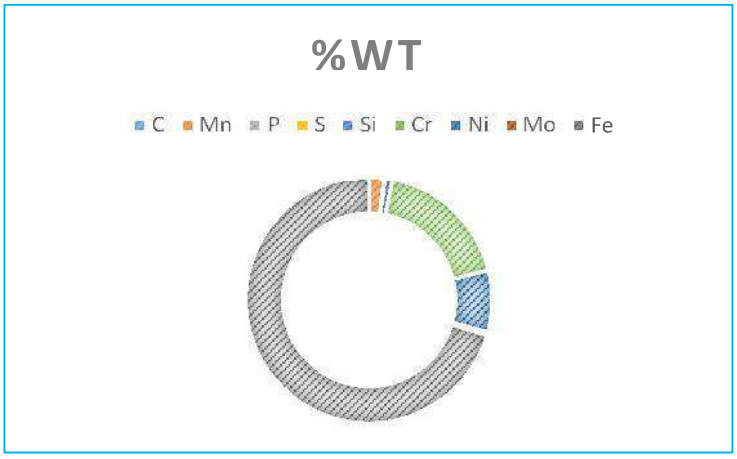

Figure 2: Chemical composition base Metal 304L stainless steel

2.2 Welding Process of ASS using TIG welding machine

The previous dimension sample sliced in to five (5) equal pieces of 60mm x 30mm x 5mm, were labelled A, B, C, D and E and further sliced in to the dimension of 30mm x 15mm x 5mm and labelled; A_1&A_2,B_1&B_2, C_1&C_2, D_1&D_2 and E_1&E_2 respectively. The samples ABCDE (1&2) were welded together at a designated welding current of 50A, 60A, 70A, 80A and 90A respectively. The corresponding welding temperature was also recorded using the K-type thermocouple digital thermometer model: HHM29. The weldments were allowed to cool gradually

under natural air conditional at room temperature. Table 2 and Table 3 Presents the TIG welding parameters used in this study. The welding conditions adopted were;

1. The weldments was cooled naturally in air so as to prevent the imposition of stress on the weld to avoid crack or avoid unnecessary vacancies (or area of defect or failure) in the weld.
2. It was ensured a narrow beads was deposited during welding
   No pre-heating of the base metal should be done to prevent martensite formation in the weld.

TABLE 2: TIG welding parameters employed for ASS 304L

Electrode	Filler metal	Current (A)	Electrode diam (mm)	Filler diam (mm)
EW-Th-2	Filler 308	50,60,70,80, 90	3.15	3.15

Table 3: Parameters of TIG welding machine used

Machine type	Model	Power (hp)	Voltage (V)	Current (A)	Frequency (Hz)	Dimension (mm)
GYS TIG 250	AC/DC–HF	3	400	5 - 250	50/60	350x640x670

2.3 Metallurgical Test

2.3.1 Macro-structure and Micro-structure Examination

Macro-structure examination was first carried out on the parental metal of ASS 304L type as well as the weldments. Grinding of each specimen was carried out using paper grit of SiC of different grades ranges from 220-800 grit. The polishing of each samples by the use of emery clothe with alumina and water were carried out in a rotating polishing machine disc. The polished samples were etched at the weld joints using stainless steel etchant in the ratio of 10ml HNO3, 30ml HCL and 10ml glycerol. The time for etching was 2min. The width of HAZ of each samples were measured with the meter rule and each of the values were recorded.

3.0 Results and Discussion

A metal plate of austenitic stainless steel (ASS) of dimension 230mm x 150mm x 5mm was used in this research work. The dimension was sliced into five (5) equal samples of 60mm x 30mm x 5mmdimensions respectively. The sliced dimensions were further sliced into 30mm x 15mm x 5mm as specified and labelled in the methodology. The weldment of the samples was carried out

to investigate at what particular welding temperature ASS will be fastened together without chromium carbide formation. The results obtained from the various welding current were tabulated in Table 4 along with the welding temperature of each of the sample A, B, C, D & E. The relationship between the welding current and welding temperature is illustrated in Figure 3.

Table 4: Result of the welding current with corresponding temperature and power

Welding process	A	B	C	D	E
Welding current	50	60	70	80	90
Welding temp(c)	100.6	200.2	300.8	400.2	500.6

From Figure 3: below, it was observed that the welding temperature rises as the values of the welding current increases. This variation in the values of welding current determines the corresponding increase in welding temperature at which the formation of chromium carbide formation is likely to form. The choice of the welding machine in Table 3 was due to the aim of achieving a particular welding temperature at which "weld decay" (i.e. a significant chromium carbide formation) can be avoided when welding ASS 304L at lower temperature and also due to the available low range of current values of the Machine. The result of width dimension of HAZ of each weldments is presented in Table 5 below.

Table 5: Width dimension of HAZ od each weldments

Width of HAZ (mm)	A	B	C	D	E
	1.0	1.2	2.2	2.7	3.2

The width of HAZ illustrates the relationship between the welding current, temperature and width dimensions as the welding current and temperature increases. Figure 4 below depicts the relationship between the three (3) parameters. It was observed that the width of HAZ of each weldment measured varied at each value of welding current and corresponding temperature from 1.0mm to 3.2mm. The weldment with lowest width dimension of HAZ (i.e. sample A) with the lowest current of 50A, has the best mechanical property of ultimate tensile strength (UTS) of a material as compared with sample E with width dimension of HAZ of 3.2mm as earlier reported by (Guo et al., 2014) in their current research that the ultimate tensile strength (UTS) of a weldment material increases when the heat input is at the lowest. The relationship between welding current, temperature and width of HAZ is presented below in figure 3.

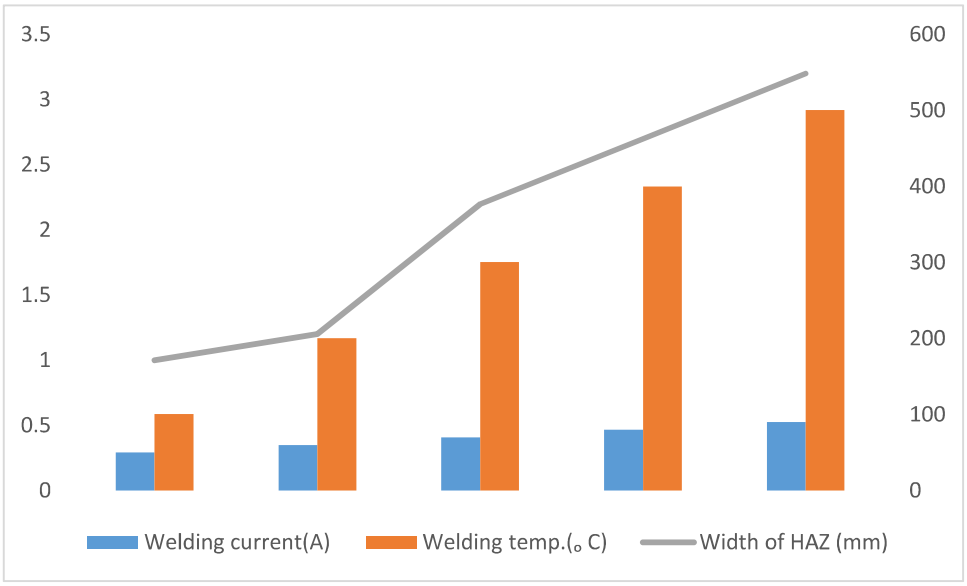

Figure 3: The relationship between welding current, temperature and width of HAZ

From Figure 3, as earlier reported by Guo et al., (2014), the ultimate tensile strength (UTS) of a weldment material increases when the heat input is at the lowest. It shows that when the heat input increases from C to E, at 2.2mm and 3.2mm with the corresponding temperature of 300.8°C to 500.6°C and current of 70A to 90A, then there is decrease in ultimate tensile strength (UTS).

The following Plates from plate 1 to Plate 6 depicts the microstructure of the parental metal used, the weldments A, B, C, D & E samples of ASS 304L type, the ASS 304L etched in a solution of 10ml HNO_3 +30ml HCL and 10ml glycerol.

3.1 Microstructure of the parental metal and the weldments

The following plates from plate 1 to plate 6 depicts the microstructure of the parental metal used, the weldments A, B, C, D & E samples of ASS 304L type, the ASS 304L etched in a solution of 10ml HNO_3 +30ml HCL and 10ml glycerol.

Plate 1: Microstructure of (as-received) of ASS 304L (Etched) using a solution of 10ml HNO3 + 30ml HCL and 10ml glycerol for 2mins.

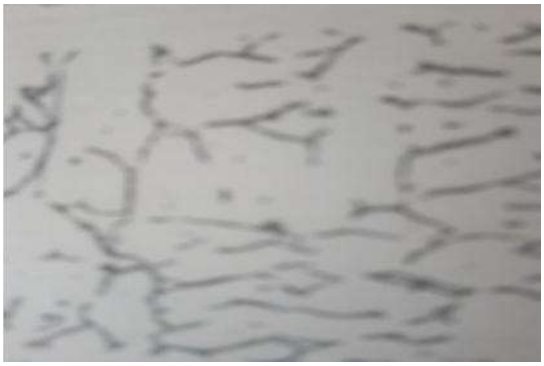

Plate 2: Micro-structure of Weldment sample A of ASS 304L (Etched) using TIG with 308 filler metal at temperature of 100.6°C cooled in air.

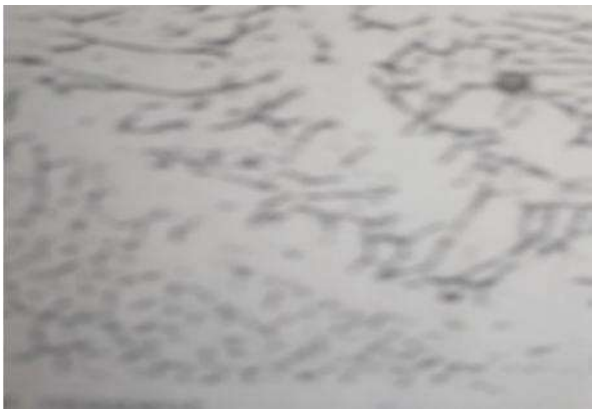

Plate 3: Micro-structure of Weldment sample B of ASS 304L (Etched) using TIG with 308 filler metal at temperature of 200.2°Ccooled in air.

Plate 4: Micro-structure of Weldment sample C of ASS 304L (Etched) using TIG with 308 filler metal at temperature of 300.8°C cooled in air

Plate 5: Micro-structure of Weldment sample D of ASS 304L (Etched) using TIG with 308 filler metal at temperature of 400.2^{o}Ccooled in air

Plate 6: Micro-structure of Weldment sample E of ASS 304L (Etched) using TIG with 308 filler metal at temperature of 500.6^{o}C cooled in air.

3.2 Micro-structural analysis of parental metal plate and the weldments

From Plate 1, the micro-structure of Parental metal Plate of ASS contains ferrite (dark) streaks in the matrix of austenite which is invulnerable by the etchant. Weldment sample A from Plate 2, just as similar to Plate 1, contains ferrite (dark) in a matrix of austenitic (white). The weldment B in Plate 3 has a structure that contains the same ferrite (dark) in a matrix of austenite, but the ferrite (dark) is more massive than in weldment A. Weldment C as shown in Plate 4, shows dendrite structure with excess delta ferrite (white). The structure also reveals chromium carbide formation of fine grained ferrite (dark) structure. In weldment D in plate 5 the structure consist of high chromium carbide formation of austenite grains precipitated at the grain boundaries. The structure also contains precipitated chromium carbide (small dark particles) in austenitic matrix as illustrated in Plate 5. The last weldment E, in Plate 6 reveals a micro-structure as same as that of sample D in Plate 5 that contains high chromium carbide formation of austenite grains precipitated at both inside and outside the grain boundaries. The structure also contains precipitated chromium carbide (small dark particles) in austenitic matrix as illustrated in Plate 5. The micro-structures reveals that: there is no chromium carbide formation in the weldment of sample A Plate 2 and

sample B Plate 3, but very obvious and significant formation of chromium carbide in weldment C Plate 4, D Plate 5 and E Plate 6.

4.0 Conclusions

The welding of ASS 304L has been carried out, using TIG welding technique. The formation of chromium carbide with increase in welding current along with the corresponding
Increase in temperature was investigated. Based on the result of macro examinations and microstructures. The following conclusions were drawn. Based on the result of micro-structures, the material of ASS of type 304L welded at lower current of 50A, 60A at a corresponding welding temperature of 100.6^{o}C and 200.2^{o}Cdo not contains chromium carbide formation in the weld. This will eventually solve the problem of corrosion due to a corrosion mechanism called weld decay in petrochemical, oil and gas, automobile, marine, robotic, aerospace and nuclear industries if a control temperature is applied.

Finally, ASS 304L type with the lowest width of HAZ (i.e. 1.0mm and 1.2mm) at a given weld current of 50, 60A with a corresponding temperature of 100.6^{o}C and 200.2^{o}C gives a better mechanical properties of strength and hardness. The experimental welding temperature commensurate with the computer simulated welding temperature, which justify the validity of weldments of austenitic stainless steel ASS 304L at lower range of temperature of 100.6^{o}C and 200.2^{o}C.

Acknowledgments
The authors acknowledge the support of Department of Materials and Metallurgical Engineering, Federal University of Technology, Minna Nigeria for providing metallurgical testing facilities.

References

Gao, X. D., and Zhang, Y. X. (2014). Prediction model of weld width during high-power disk laser welding of 304 austenitic stainless steel. International journal of precision engineering and manufacturing, 15(3), 399-405.

Guo, J. F., Chen, H. C., Sun, C. N., Bi, G., Sun, Z., & Wei, J. (2014). Friction stir welding of dissimilar materials between AA6061 and AA7075 Al alloys effects of process parameters. Materials & Design (1980-2015), 56, 185-192.

Joo, S. M., Bang, H. S., Bang, H. S., and Park, K. S. (2016). Numerical investigation on welding residual stress and out-of-plane displacement during the heat sink welding process of thin stainless Steel Sheets. International Journal of Precision Engineering and Manufacturing, 17(1), 65-72.

Mendes, R., Ribeiro, J. B., and Loureiro, A. (2013). Effect of explosive characteristics on the explosive welding of stainless steel to carbon steel in cylindrical configuration. Materials & Design, 51, 182-192.

Mishra, D., Vignesh, M. K., Raj, B. G., Srungavarapu, P., Ramkumar, K. D., Arivazhagan, N., and Narayanan, S. (2014). Mechanical characterization of Monel 400 and 316 stainless steel weldments. Procedia Engineering, 75, 24-28.

Moslemi, N., Redzuan, N., Ahmad, N., and Hor, T. N. (2015). Effect of current on characteristic for 316 stainless steel welded joint including microstructure and mechanical properties. Procedia CIRP, 26, 560-564.

Oyetunji, A., Kutelu, B. J., and Akinola, A. O. (2013). Effects of Welding Speeds and Power Inputs on the Hardness Property of Type 304L Austenitic Stainless Steel Heat-Affected Zone (HAZ). Journal of Metallurgical Engineering, 2(4), 124-129.

Reddy, M. P., William, A. A. S., Prashanth, M. M., Kumar, S. S., Ramkumar, K. D., Arivazhagan, N., and Narayanan, S. (2014). Assessment of Mechanical Properties of AISI 4140 and AISI 316 Dissimilar Weldments. Procedia Engineering, 75, 29-33.

Roy, C., Pavanan, V. V., Vishnu, G., Hari, P. R., Arivarasu, M., Manikandan, M., and Arivazhagan, N. (2014). Characterization of metallurgical and mechanical properties of commercially pure copper and AISI 304 dissimilar weldments. Procedia Materials Science, 5, 2503-2512.

Song, E. J., Baek, S. W., Nahm, S. H., and Baek, U. B. (2017). Notched-tensile properties under high- pressure gaseous hydrogen: Comparison of pipeline steel X70 and austenitic stainless type 304L, 316L steels. International Journal of Hydrogen Energy, 42(12), 8075-8082.

Yang, J., Xiao, B. L., Wang, D., & Ma, Z. Y. (2010). Effects of heat input on tensile properties and fracture behavior of friction stir welded Mg–3Al–1Zn alloy. Materials Science and Engineering: A, 527(3), 708-714.

Zhang, M., Chen, G., Zhou, Y., and Liao, S. (2014). Optimization of deep penetration laser welding of thick stainless steel with a 10 kW fiber laser. Materials & Design, 53, 568-576.